JOURNAL OF GEOPHYSICAL RESEARCH, VOL. 100, NO. C10, PAGES 20,793–20,804, OCTOBER 15, 1995

Trapped, near-inertial waves and enhanced chlorophyll distributions

T. Granata,[1] J. Wiggert, and T. Dickey

Ocean Physics Group, Department of Earth Sciences, University of Southern California, Los Angeles

Abstract. Waves with near-inertial frequencies were observed along a front associated with a large mesoscale feature in the Sargasso Sea during the late summer of 1987. High subsurface chlorophyll concentrations occurred on the edge of this front, coincident with the wave packets. The amplitude of the waves increased with time, and kinetic energy propagated downward, reducing 20-m Richardson numbers in the thermocline to 1 or less. Chlorophyll levels were episodic, showing no periodicity coincident with wave dynamics. However, on two occasions, chlorophyll concentration increased from <0.5 to >1 mg Chl m^{-3}, several hours after the waves penetrated the thermocline. It was hypothesized that mixing associated with shear instabilities stimulated new production. A diffusivity model combined with nutrient data produced a phytoplankton bloom that accounted for only one of the maxima. The other increase in chlorophyll may have been the result of horizontal advection of the wave packets near the front.

1. Introduction

It has been hypothesized that large, vertical shears caused by near-inertial waves can elevate mixing levels in the water column [*Gregg et al.*, 1986]. Large-amplitude near-inertial waves have been reported along frontal regions in the ocean [*Weller*, 1982, 1985; *Kunze and Sanford*, 1984; *Mied et al.*, 1986; *Weller et al.*, 1991; *Salat et al.*, 1992]. One hypothesis proposed to explain the occurrence of near-inertial waves along a front is that of wave trapping [*Kunze and Sanford*, 1984; *Kunze*, 1985]. Two mechanisms can trap waves within a front. First, the mean flow of the front can Doppler shift waves toward the inertial frequency. Second, relative vorticity changes within the front modulate the lower-frequency bound of the inertial waveband, i.e., the range of allowed inertial wave frequencies. Waves are not trapped uniformly across a front, but rather, are asymmetrically distributed across the front for the second mechanism. On the cold side of a front, in regions of positive relative vorticity, oscillations will be higher than f, the frequency resulting from Coriolis motion, while on the warm side of a front, in regions of negative relative vorticity, frequencies will be lower than f [*Kunze*, 1985].

While many physical studies have been devoted to the dynamics of near-inertial waves, biological observations are few. In coastal areas, wave-chlorophyll interactions have been studied for a variety of other wave types, including high-frequency internal waves [*Haury et al.*, 1983], semidiurnal and diurnal tides [*Lafleur et al.*, 1979], and deep ocean solitons [*Holligan et al.*, 1985]. More recently, *Franks* [1995] has simulated the effect of near-inertial waves on a vertical chlorophyll distribution. The variability of primary production within the deep chlorophyll maximum has been attributed to wave-induced diffusion of nutrients from below the nitracline [*Armstrong and La Fond*, 1966; *Pingree and Mardell*, 1981]. Diffusion of nutrients across isopycnal boundaries is slow but may be enhanced by breaking waves which would increase turbulent mixing [*Gargett and Holloway*, 1984; *Denman and Powell*, 1984]. *McGowan and Hayward* [1978] observed subsurface temperature anomalies and mixed layer deepening, coincident with increased primary and secondary production in the central gyre of the North Pacific. They suggested that breaking waves mixed limiting nutrients into the euphotic zone, causing episodic fertilization events which stimulated production. Another wave mechanism that could stimulate primary production is wave pumping of nutrients into the euphotic zone [*Kahru*, 1983]. This would occur when isopycnal surfaces containing phytoplankton and nutrients are periodically displaced upward in the euphotic zone. Theoretical studies have suggested that waves with periods similar to the growth cycles of phytoplankton would enhance photosynthetic activity as the crest of a wave lifts cells into higher light regimes [*Kamykowski*, 1974, 1976].

During the late summer of 1987 a large frontal system advected through the Biowatt II mooring site in the Sargasso Sea. Associated with the front were near-inertial wave packets and elevated chlorophyll concentrations. In this paper we first examine how these waves were formed and then investigate if and how wave dynamics could have enhanced chlorophyll levels near the front.

2. Methods

Time series were collected from a mooring during the Biowatt II experiment in the Sargasso Sea (34°N, 70°W). The data collected from two of three mooring deployments spanned Julian days 230-242 and 245-270, corresponding to August 18-September 27 of 1987 [*Dickey et al.*, 1991, 1993]. Multivariable moored systems (MVMS) were deployed below a surface meteorological buoy at nominal depths of 10, 20, 40, 60, 80, 100, 120, and 160 m. Data for horizontal currents (u, v components), temperature, fluorescence, and photosynthetically available radiation (PAR) were averaged

[1]Now at Centro de Estudios Avanzados de Blanes, CSIC, Blanes, Spain.

Paper number 95JC01665.
0148-0227/95/95JC-01665$05.00

and recorded every 4 min at each depth [*Dickey et al.*, 1993]. Measurements of barometric (atmospheric) pressure, wind speed, and wind direction were taken every 7.5 min from meteorological sensors located on the surface buoy, 3 m above the ocean surface. Prior to deployment, chlorophyll fluorescence (chl fluorescence) was calibrated against extracted chlorophyll using laboratory cultures [*Marra et al.*, 1992]. Water samples for nitrate analyses were collected between mooring deployments from August 22 to 26. For a complete list of other parameters sampled and a description of the MVMS, see *Dickey et al.* [1993].

Wave motions were evident for high-frequency data, while frontal and mesoscale features were more evident at subinertial frequencies. Data were treated differently to separate trends in mesoscale variability from wave dynamics. Low-frequency averages were formed from broadband data passed through a 76-hour Gaussian filter. This removed diel, inertial, and higher-frequency signals and emphasized the synoptic nature of the front. Higher-frequency data, averaged to 1-hour bins, resolved near-inertial motions in the time series. Color, depth-time distributions of chl fluorescence, temperature, and north velocity (Plate 1) were produced by fitting a cubic spline curve to the 1-hour averages, interpolating the function from 10-160 m in increments of 0.6 m.

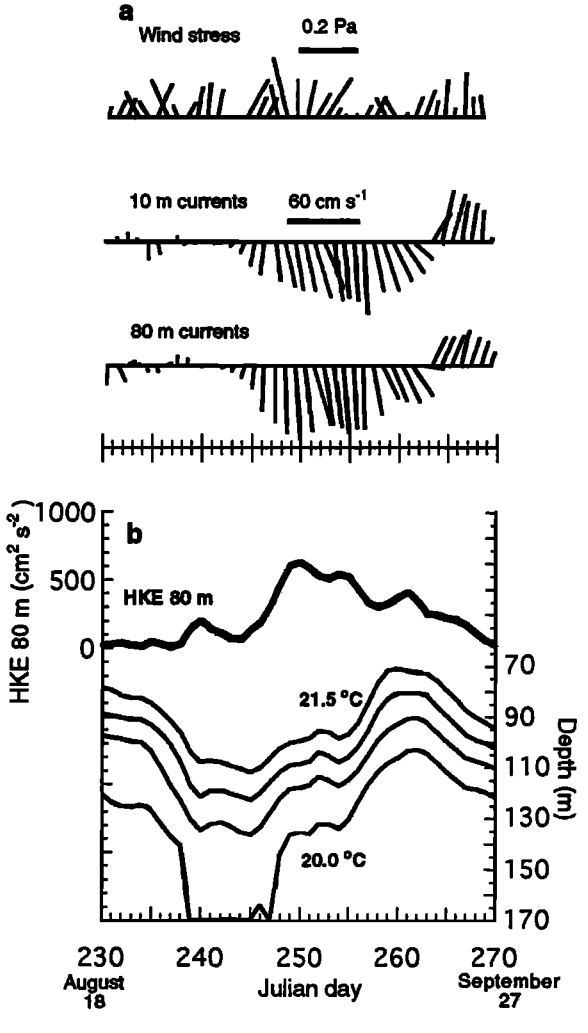

Figure 1. A subinertial time series of (a) wind stress and 10- and 80-m current vectors; and (b) 80-m horizontal kinetic energy (HKE) (thick line) and depths of upper ocean isotherms (thin lines). Data corresponding to day 243 are missing because no mooring was in the water during this period.

Since no coincident salinity data were available, a temperature-density relationship was compiled from *Levitus* [1982] and used to convert temperature time series to densities. The mesoscale front cited in this paper was the result of a Gulf Stream meander pinching off Sargasso Sea water [*Dickey et al.*, 1993]; thus we have the following two water masses: Sargasso Sea and Gulf Stream. The temperature-density relationship may not hold if mesoscale fronts with different salinity-temperature, and thus density-temperature, relationships advect into the site. However, for the vertical temperature gradients in this paper the density differences in Gulf Stream water were no more than 0.25 kg m^{-3}, based on climatological data [*Watts*, 1983, Figure 10]. Thus, we will assume that the temperature-density relationship accounts for both local and mesoscale conditions.

The buoyancy frequency (N^2) was calculated from density estimates as $(g/\rho_0)(\Delta\rho/\Delta z)$, where g is gravitational acceleration, $\Delta\rho/\Delta z$ is the vertical density gradient, and ρ_0 is the average density between depths of Δz. Vertical shear was calculated as $[(\Delta u/\Delta z)^2+(\Delta v/\Delta z)^2]^{1/2}$. Because buoyancy frequency and shear were calculated from instruments 20 m apart, we could only estimate a coarse 20-m Richardson number, $Ri=N^2\{[(\Delta u/\Delta z)^2+(\Delta v/\Delta z)^2]^{1/2}\}^{-2}$. Shear and buoyancy frequency were calculated from full bandwidth data, then filtered, and averaged to 1-hour bins. Buoyancy frequency was low-pass filtered, with a 0.03 cph cutoff. Two shear data sets were generated, one using the low-passed filter and the other using a band-passed filter of 0.038 to 0.061 cph, which was centered on f, the local inertial frequency.

For spectral plots, fast Fourier transforms were computed after mean trends were removed from an 18-day time series (Julian days 245-263) and a 50% cosine taper applied. Autospectra of currents were calculated from rotary spectra following *Gonella* [1972]. Rotary spectra partitioned the time series into clockwise and anticlockwise components which represented the turning of vectors with time.

3. Observations

Using images of sea surface height and National Oceanic and Atmospheric Administration (NOAA) sea surface temperature maps, *Dickey et al.* [1993] have observed that a mesoscale frontal system was in the vicinity of the Biowatt II mooring site from mid-August to mid-September of 1987 (Julian days 233-260). The mesoscale front appeared to be associated with an outbreak of warm, Gulf Stream water which entrained cooler Sargasso Sea water. The cooler water formed the center of an eddy, with warmer waters along the perimeter forming a convoluted front.

Figures 1a and 1b show subinertial distributions of wind stress, 10- and 80-m current vectors, 80-m horizontal kinetic energy (HKE), and isotherm depths (from 70-170 m) during the passage of the front. The frontal system was extremely dynamic as characterized by the time series of rotating current vectors (Figure 1a) and of deepening and shallowing isotherms (Figure 1b). Initially, currents speeds were low. From days 248-258, currents speeds reached 80 cm s^{-1}, with daily averaged speeds of 40-60 cm s^{-1} directed to the southeast and to the south. By day 259, current velocities decreased and

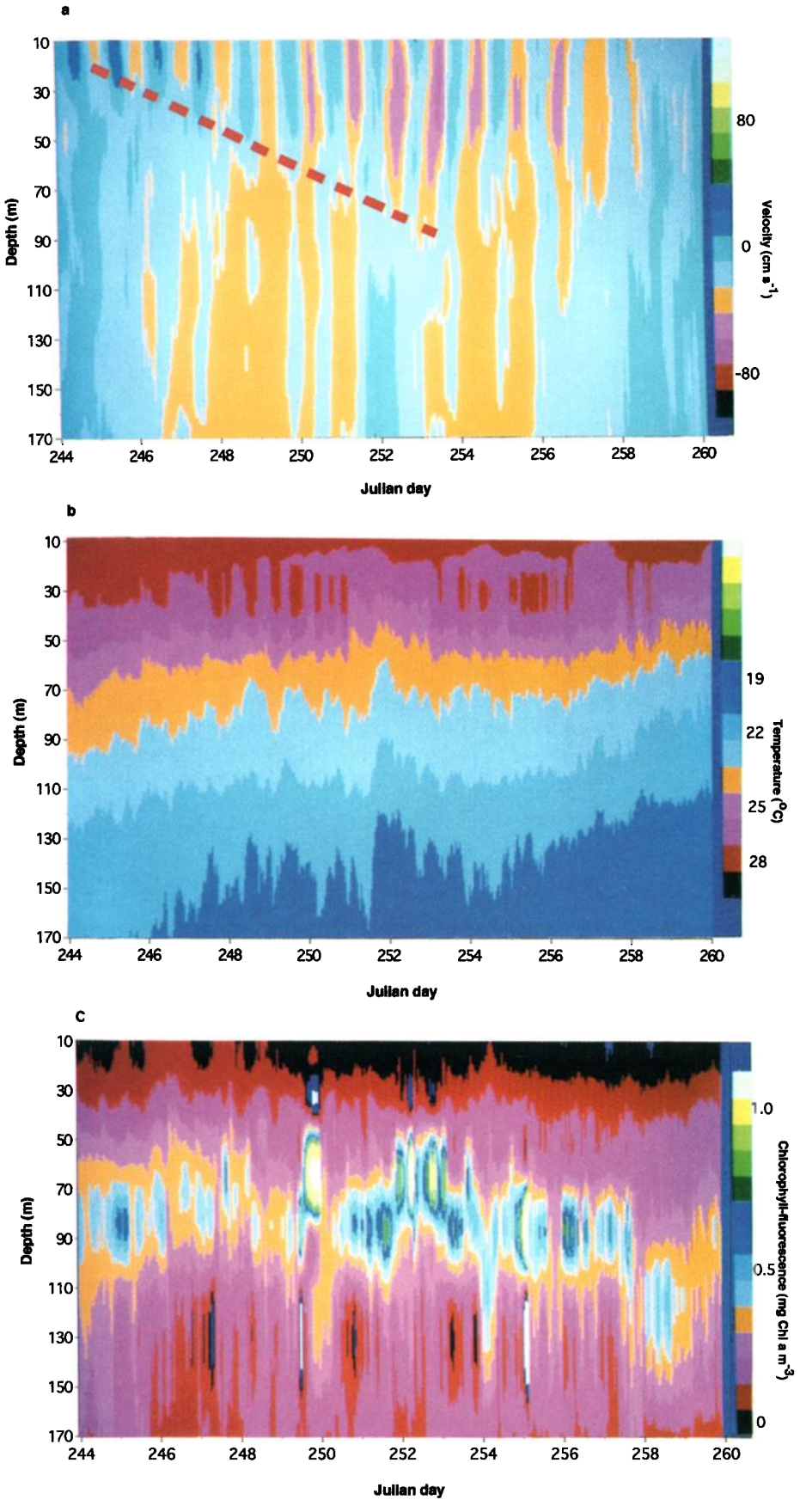

Plate 1. Depth-time distributions of (a) the north velocity component, v, (b) temperature, and (c) chlorophyll fluorescence. Magnitudes of each scalar quantity are given in the color scale on the right-hand side and were calculated from raw data averaged to 60 min and interpolated every 0.6 m over depth.

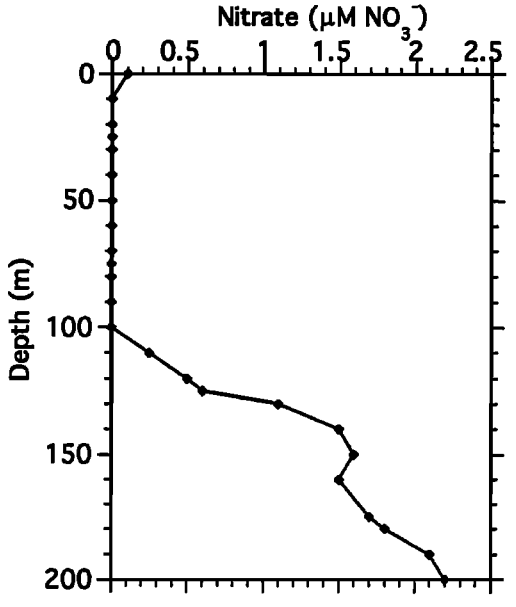

Figure 2. A profile of the nitrate concentration at the mooring site on day 243.

changed direction to the southeast and eventually to the northeast. Surface wind stress was variable, primarily from the southwest and the southeast with average magnitudes <0.15 Pa and a maximum of 0.21 Pa (Figure 1a).

Generally, isotherms deepened from days 230 to 241, remained fairly constant for 2 days, then began to gradually shoal from days 245 to 255 (Figure 1b). Days 244 to 255 showed high horizontal kinetic energy; this was the period when wave packets were observed on the warm side of the front.

The high-frequency time series are shown in Plates 1a-1c. Near-inertial waves can be seen in Plate 1a. Oscillations in wave speed are shown as alternating color bands. The inertial frequency at this site was 0.0466 cph, so a complete wave cycle occurred approximately once every 21.5 hours. Wave speed increased with both time and depth, propagating wave energy into the thermocline. The group velocity of the wave C_{gz}, which represents the downward rate of energy propagation, was graphically estimated to be 6.1 m d^{-1} from Plate 1a. Inertial motions propagated from the surface waters into the thermocline and were not evident below 80 m until day 252.

Isotherm distributions showed a return to cooler water conditions (< 20°C) toward the end of the time series (Plate 1b). The largest high-frequency, vertical fluctuations in isothermal depths coincided with oscillations of near-inertial waves. Ascending isotherms occurred on days 248.4, 249.4, and 251.8 and are evident from the motion of the 24°C isotherm (the gold band) in Plate 1b. Isotherms were uplifted for durations of approximately 7-12 hours as inertial energy penetrated to depths greater than 90 m.

The highest chl fluorescence values were found below the mixed layer. Throughout the time series the deep chlorophyll maximum (DCM) was located between 50 and 90 m (Plate 1c), while the depth of the nitracline was between 100 and 110 m (Figure 2). The depth of the 1% PAR was also between 100 and 110 m from days 245 to 260 [*Dickey et al.*, 1993]; thus the DCM was in the euphotic zone and just above the nitracline the entire time the front was present. Between days 245 and 249.5, subsurface chl fluorescence levels between 10 and 160 m had a maximum of only 0.56 mg Chl *a* m^{-3} located at 80 m. However, episodic peaks >1.3 mg Chl *a* m^{-3} occurred from days 249.5 to 250 and 252.2 to 254 and were located between 50 and 80 m. Areal chl fluorescence, defined as

$$\int_{10m}^{160m} Chla \; dz,$$

was highest from days 249.5 to 255.5 (Table 1).

Inertial periodicity in rotary current spectra was confined to clockwise (CW) rotation. A sharp peak near the inertial frequency was present in the 10-m CW spectrum. Near-inertial peaks became smaller and broader at 40 and 60 m (Figure 3a). Below 80 m, peaks were not significant. Temperature autospectra had small inertial peaks from 40 to 80 m. However, these were not statistically significant (Figure 3b). Similarly, chl fluorescence had no significant signal near the inertial frequency at 40, 60, or 80 m (Figure 3c). Thus, while currents in the upper portion of the water column showed inertial periodicity, deeper currents did not nor did temperature or chl fluorescence.

Subinertial buoyancy frequency was highest between 30 and 110 m (Figure 4a). Above 30 m, N increased near day 250 which would account for higher near-inertial energy based on WKB scaling [*Munk*, 1981]. Below 30 m, N decreased slightly. The subinertial scale was chosen since buoyancy frequency is controlled by mesoscale (i.e., low frequency) variability. Although subinertial shear was highest in the surface layers and generally decreased over depth, a secondary peak occurred in the pycnocline from days 252 to 254 (Figure 4b). The near-inertial shear was highest in the pycnocline (Figure 4c). The highest values of near-inertial shear occurred before day 248 and near day 252. Near-inertial shear was greater than or the same order of magnitude as the subinertial shear in most cases. The possibility that shears were unstable over tens of meters was investigated by plotting 20-m Richardson numbers in the thermocline (Figure 5). The 20-m Ri were reduced to $O(<1)$ throughout the water column around days 252-253. The 20-m Ri reflect the decrease in N and increase in near-inertial (and subinertial) shear.

4. Discussion

Dickey et al. [1993] have shown that fronts and mesoscale eddies were common features near the mooring site and that a

Table 1. Chlorophyll Fluorescence Changes During the Passage of the Front From Julian Days 245 to 262

Chllorophyll Maxima	JD 245-249.5	JD 249.5-255.5	JD 255.5-262
Chlorophyll, mg Chl *a* m^{-3}	0.56 (80 m)	1.4 (50 m)	0.68 (80m)
Areal chlorophyll, mg Chl *a* m^{-2}	32.6 ± 2.9	35.2* ± 4.9	28.3± 2.4
Sample size	113	144	178

The numbers in parentheses indicate the depth of the chl fluorescence maximum.

*Here the probability is p≤ 0.0001 based on a general linearized model with interactions. The F statistic is F=1947 and the total sample size is 435.

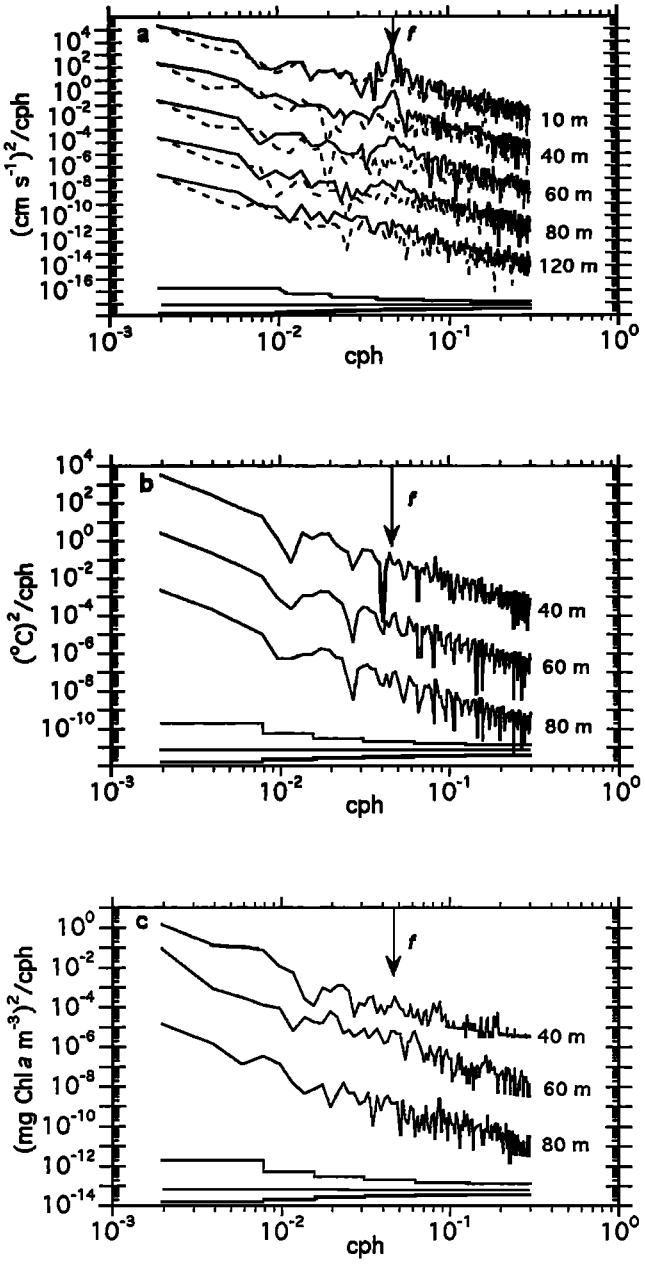

Figure 3. (a) Rotary spectra for currents, with solid lines showing clockwise and dotted lines, anticlockwise, components. (b) Autospectra for temperature. (c) Autospectra for chlorophyll fluorescence. Spectra were offset by 10^3 from the top spectra to facilitate comparisons. The arrow indicates the inertial frequency f (0.0466 cph). The 95% confidence levels are shown at the bottom.

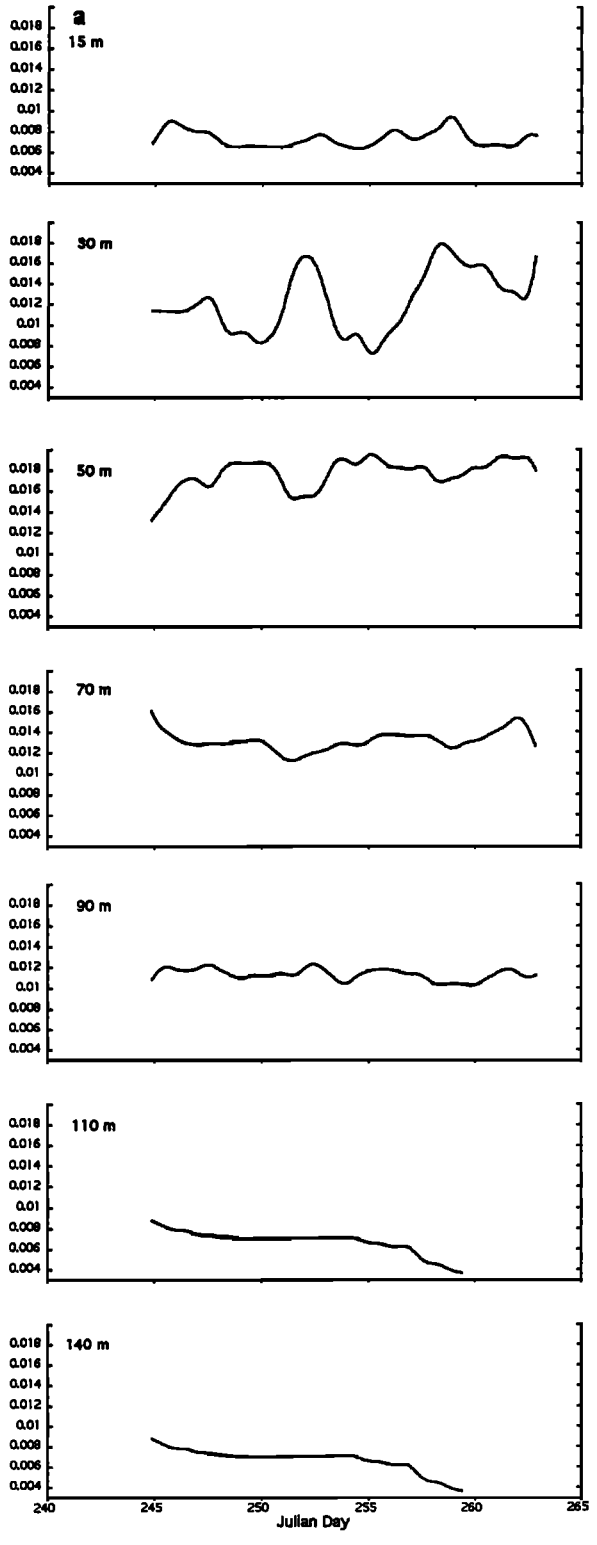

Figure 4. Time series as a function of depth for (a) low-passed buoyancy frequency N, (b) low-passed shear, and (c) band-passed shear. Data were averaged to 1-hour bins.

warm frontal system was near the site in the late summer of 1987. In situ, subinertial temperature and current data confirm the presence of this warm water, dynamic front at the mooring site from days 244 to 258. Superimposed on the large-scale dynamics along the warm side of the front were higher-frequency fluctuations dominated by near-inertial motions. First, we will investigate the probable cause of the wave field and then return to biological forcing of the chlorophyll distributions.

4.1. Forcing of Inertial Waves

Kunze and Sanford [1984] discussed three possible mechanisms for the production of high-energy inertial waves

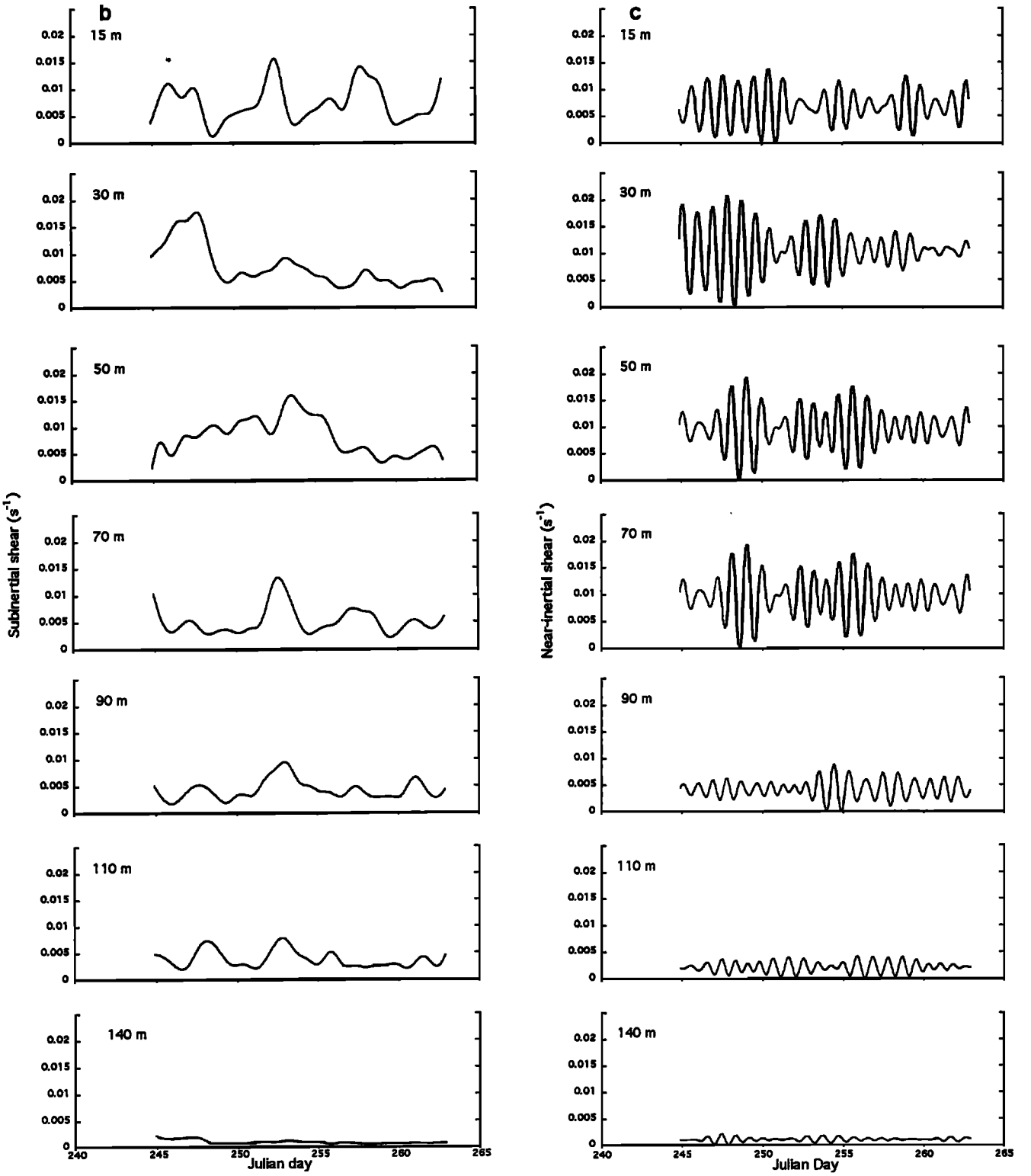

Figure 4. (continued)

in the open ocean as follows: (1) geostrophic adjustment caused by barotropic and baroclinic instabilities, (2) intense wind events either on spatial scales of $O(10$ km) or which reduce oceanic wave scales, and (3) wave-mean flow interactions in which trapped near-inertial waves accumulate in frontal jets. On the basis of the data collected during Biowatt II, it is not possible to definitely determine which mechanism produced the high-energy inertial wave activity. We can, however, identify those mechanisms that are least consistent with our data.

Geostrophic adjustment is a possible mechanism because the frontal system was evolving from an instability in the Gulf Stream. However, isotherms along the front remained at a nearly constant depth as wave energy peaked from days 248 to

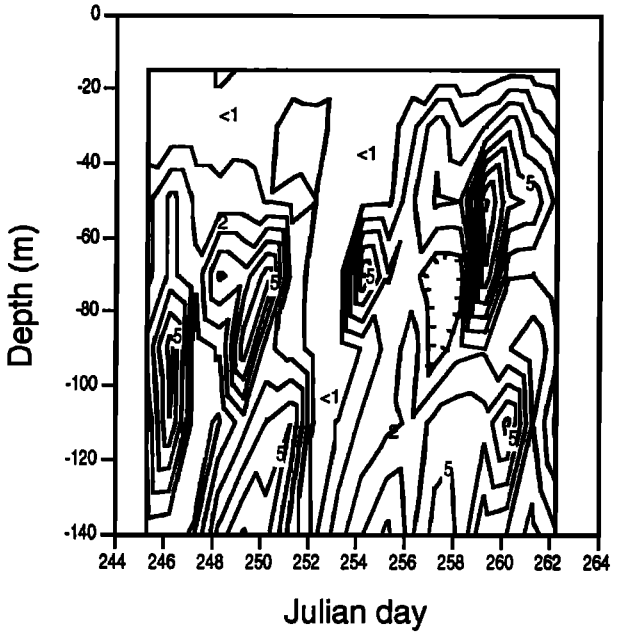

Figure 5. Depth-time distributions of 20-m Richardson numbers (20-m Ri) calculated from subinertial N and broadband shear.

255, which seems inconsistent with theories of baroclinic instabilities forcing inertial waves.

Models of *Kundu and Thompson* [1985] and *Eriksen* [1988] demonstrated that inertial waves could be generated by wind events along moving atmospheric fronts. Wind could have generated high-energy inertial waves if high wind stress occurring during the passage of a low-pressure storm system (Tables 2a and 2b) transferred energy into the upper ocean. To determine the effect of wind on near-inertial motions in the mixed layer, the model of *Pollard* [1970] was used,

$$\frac{\partial u}{\partial t} = \frac{\tau_x}{H\rho} + fv - cu \qquad (1a)$$

$$\frac{\partial v}{\partial t} = \frac{\tau_y}{H\rho} - fu - cv \qquad (1b)$$

The u, v velocities were forced by hourly time series of mixed layer depth H and wind stress components τ_x and τ_y. The mixed layer was consistently near 20-25 m. The wind stress coefficients were based on wind speed and air-sea potential temperature differences [*Smith*, 1988]. The damping term c was set to 0.25 d^{-1} [*Weller et al.*, 1991]. The model was solved by the Runge-Kutta scheme with a 1-hour time step. This model generates a slablike response of horizontal currents in the mixed layer which we have represented as amplitudes $[(u^2 + v^2)^{1/2}]$. Figure 6 shows time series of north and east wind stress, modeled amplitudes, and amplitudes measured by the 20-m sensor. Winds were variable in speed and direction (Table 2a), with wind stress peaking on days 244.6, 245.8, 247-249, 252.5, and 258.3. Low-passed, model amplitudes never surpassed 30 cm s^{-1}, while 20-m amplitudes increased from 10 to 42 cm s^{-1} in less than 10 days. Both modeled and measured currents peaked around day 252, coincident with the high subinertial shear. Near-inertial, modeled amplitudes initially peaked at 10 cm s^{-1} but by day 247, had decreased to <4 cm s^{-1}. The observed (20 m), near-inertial amplitudes increased from 4 to 25 cm s^{-1} and remained high until day 255. Because

Table 2a. Statistics for Atmospheric Conditions Corresponding to the Passage of the Front

Characteristics	JD 245-253	JD 254-262
Mean wind speed, m s^{-1}	7.9 ± 3.0	4.4 ± 2.5
Wind direction (from)	SE-SW (clockwise)	SE-SW (variable)
Mean wind stress, Pa	0.09 ± 0.05	0.03 ± 0.04
Mean barometric pressure, mb	1018.5 ± 2.5	1014.3 ± 0.3

Table 2b. Statistics for Oceanic Conditions Corresponding to the Passage of the Front

Variable	JD 245-258
$\overline{V_{wave}}$ at 10 m, cm s^{-1} *	22.6 ± 9.98
Mean HKE $\langle HKE \rangle$, J m^{-3} †	59 ± 29
Mean vertical energy flux, F, W m^{-2} ‡	4.2 ± 2.0 x 10^{-3}
C_{gz}, m d^{-1} §	6.1

* $\overline{V_{wave}} \int_t (u^2+v^2)^{1/2}\,dt / \int_t dt$.

† $\langle HKE \rangle = 1/2 \int_t \int_z (u^2+v^2)\,dz\,dt / \int_t \int_z dz\,dt$ for $10 \le z \le 160$ m.

‡ Flux is estimated as $F \approx C_{gz} \langle HKE \rangle$ [*Kunze and Sanford*, 1984].

§ C_{gz} the group speed, was estimated from the linear curve in Plate 1a.

modeled data were consistently lower than observed currents, yet at times were significant, we conclude that wind forcing probably played some role in the generation of the wave field, but it was not likely the sole or even main source of the inertial waves.

The last mechanism to account for the increase in near-inertial energy associated with the front is the trapped wave theory. *Kunze and Sanford* [1984], *Kunze* [1985], and *Mied et al.*, [1986] observed that wave trapping accounts for amplification of near-inertial wave energy on the warm side of fronts where negative vorticity exists. This mechanism is very effective at trapping downward propagating energy. The following characteristics were observed at the mooring site when the front was present. First, near-inertial waves were only evident in warmer water on days 245-258. The waves quickly decayed as cooler water advected into the site. Second, near-inertial energy was amplified as waves propagated downward into the thermocline. The vertical flux of near-inertial energy (4.2 x 10^{-3} W m^{-2} from Table 2b) was near the value of 4.0 x 10^{-3} W m^{-2} found by *Kunze and Sanford* [1984] for trapped waves along a subtropical front. Lastly, to determine the effect of the front on wave frequency, 10-m current phase was calculated as $(\pi/2)$-$\tan^{-1}(-u/v)$ [*Chereskin et al.*, 1989] for periods when the front slowly passed the mooring. Phase changes were calculated from full bandwidth data in order to represent both near-inertial and subinertial (frontal) effects. Figure 7 shows that wave frequencies were below f on the warm side of the front and above f on the cooler side of the front. This is consistent with changes in the effective Coriolis frequency felt by the wave packets for relative vorticity changes. On the basis of these observations, the intermittent

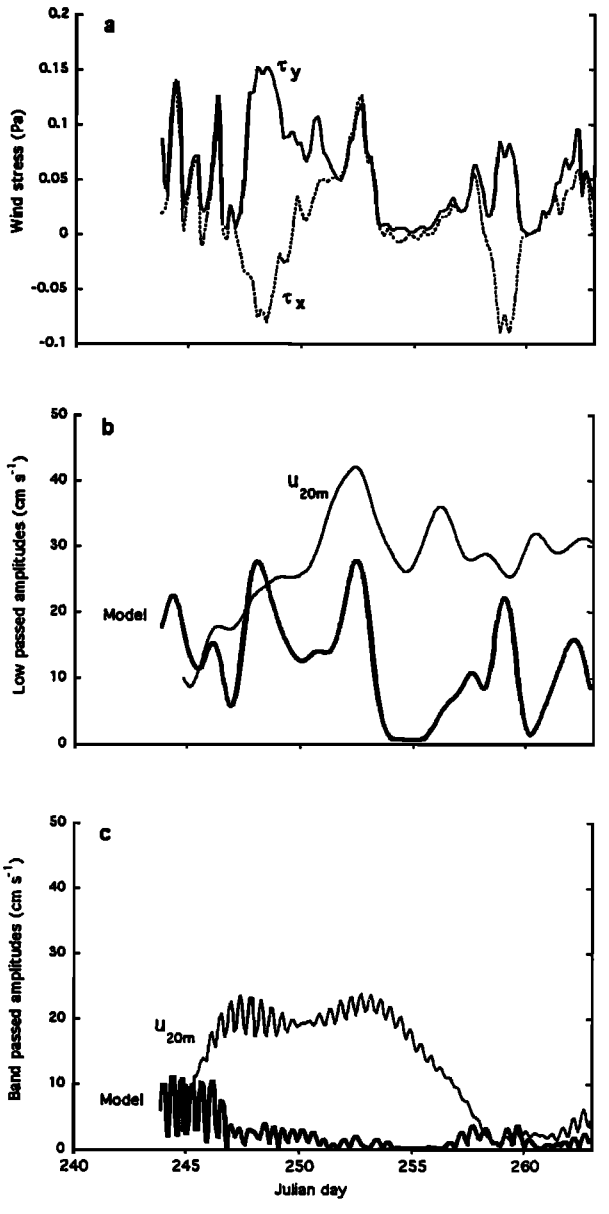

Figure 6. (a) Broadband wind stress components τ_x and τ_y, (b) subinertial amplitude from *Pollard* [1970] model and for observed 20-m currents, and (c) near-inertial amplitude from Pollard model and for observed 20-m currents.

appearance of the near-inertial wave packets appears to be most consistent with the theory of waves trapped along a front [*Mooers*, 1975a,b; *Weller*, 1982; *Kunze*, 1985]. This is not inconsistent with wind forcing, in that wind stress could have set up the wave motion, initially, and frontal currents could have modified the wave field.

4.2. Biological Forcing

The DCM showed two broad peaks in chl fluorescence between 50 and 80 m as wave energy propagated downward. Plausible explanations commonly attributed to increased chl fluorescence are as follows: physical accumulation of cells along convergent zones, photoadaptation of phytoplankton, horizontal and vertical advection of higher chlorophyll concentrations, and growth of phytoplankton.

Accumulation of chlorophyll-containing cells along the front might explain peaks in the chl fluorescence distribution [*Stommel*, 1949; *Franks*, 1992]. We note that convergent and divergent zones along fronts may be highly variable if the fronts are convoluted [*Eriksen et al.*, 1991]. While geostrophic currents, based on altimeter data, were available to us, their spatial resolution was ≈50 km, insufficient for resolving convergent-divergent features of the flow field. However, we do know that dominant chlorophyll-containing organisms during this period were mainly picoplankton [*Dickey et al.*, 1993] with limited to no swimming capabilities and near-zero sinking rates. On the basis of the model of *Franks* [1992], these types of cells would be evenly dispersed in divergent and convergent zones, and thus accumulation of cells is probably not a viable mechanism to account for the increased chlorophyll levels near days 249.5-254.

Photoadaptation of cells, which accounts for increased concentration of chlorophyll per cell, is not consistent with our data. Cells were present in higher light regimes for periods of days, which should have reduced, not increased, packaging effects.

The possibility that chl fluorescence peaks were the result of fine scale, vertical patchiness that moored sensors could not resolve, O(<20m), was also considered. A large fluorescence signal would have occurred if layers containing high chlorophyll concentrations were initially located above or below the depths of the fluorometers and then were displaced into the path of the sensors as waves pumped isotherms upward and downward. However, comparisons of chl fluorescence profiles with 1-m resolution, taken from conductivity-temperature-depth (CTD) casts near the mooring, showed chlorophyll concentrations varying gradually with depth and doubling only on scales >100 m. Over a vertical distance of 20 m, the average distance between fluorometers, patchiness in profiles could account for no more than 22% of the increased chl fluorescence found in the front.

Growth of cells could have increased chl fluorescence, especially considering that the nitracline was near 100 m and

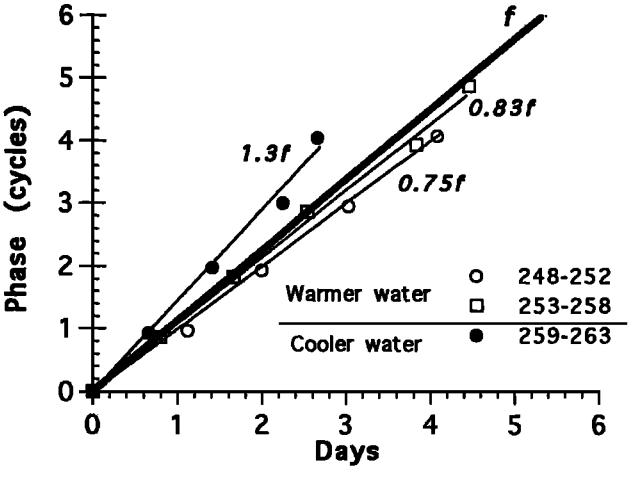

Figure 7. Phase shift of 10-m current showing the frequencies of waves relative to the inertial frequency f (illustrated by the thick line). Phase was calculated as $(\pi/2)$-$\tan^{-1}(-u/v)$ for full-bandwidth data to illustrate the effect of the front (the subinetial effect) on wave periodicity.

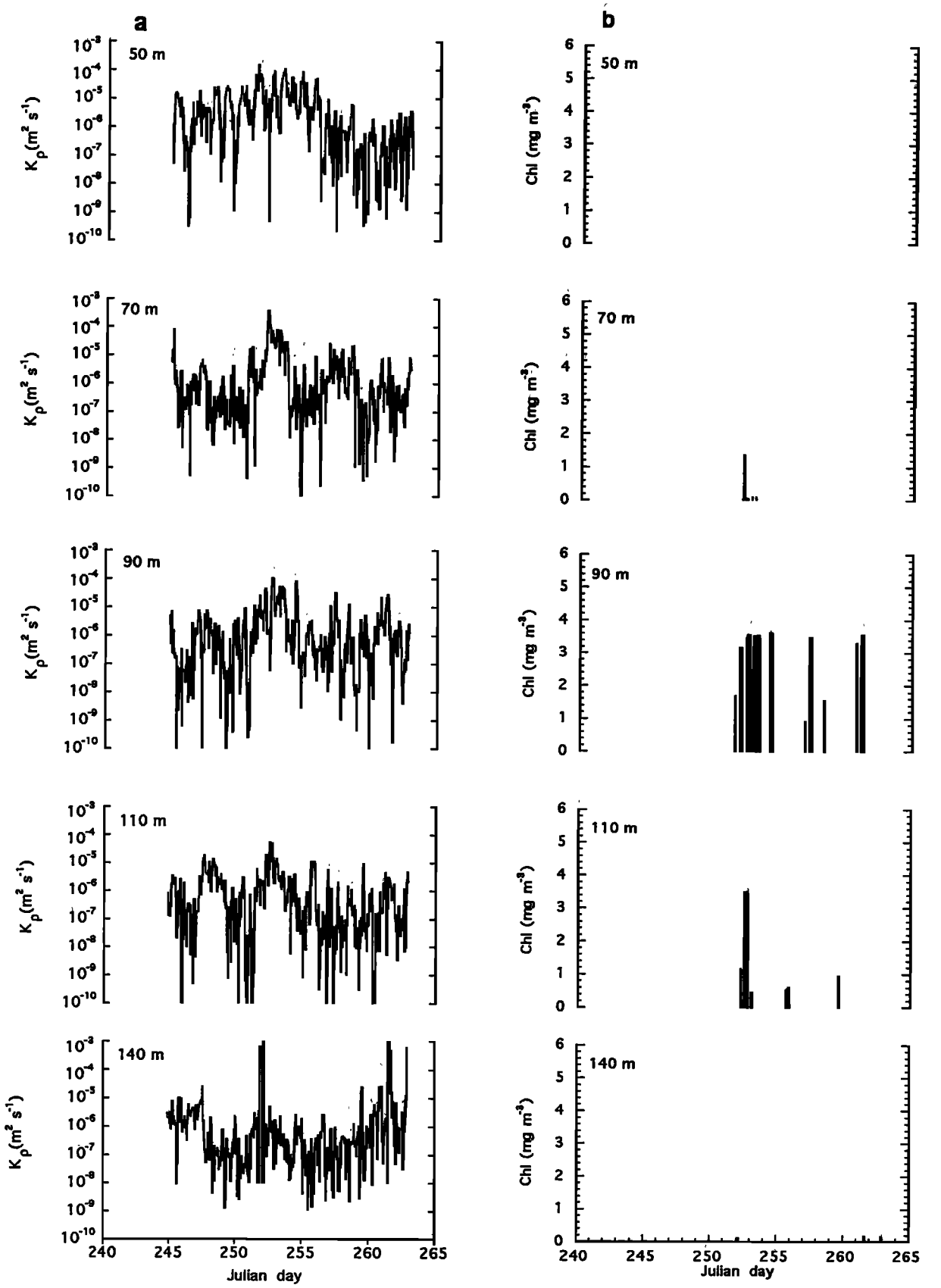

Figure 8. (a) Turbulent mixing coefficients calculated using the *Gregg* [1989] model and (b) chlorophyll concentrations based on nitrate mixing into the euphotic zone.

the depth of the euphotic zone (1% PAR) was near 110 m. It is generally accepted that phytoplankton growth rates during bloom conditions can reach 1-2 d^{-1}. Phytoplankton growth was estimated in two ways. The first method was to determine instantaneous growth rates based on $(1/\langle P\rangle)(\partial P/\partial t)$, where P is chl fluorescence biomass and $\langle P\rangle$ is the average biomass. This was a poor method since the chl fluorescence time series was not smooth, and thus the derivative was rather noisy. Still, maximum growth rates of ≈1.9 d^{-1} were estimated for the two chlorophyll increases on days 249.5 and 252. All other values were extremely low. Absolute values of negative growth rate, or the loss rate, were of the same magnitude as nominal, positive growth rates. A second estimate of growth was based on the conversion of nitrogen to chlorophyll biomass as a function of nitrogen flux into the euphotic zone. The nitrogen flux was modeled as the diffusion equation, $(\partial N/\partial t)=K_\rho(z)\,(\partial^2 N/\partial z^2)$ where $K_\rho(z)$ is a parameterization of turbulent diffusivity in a thermocline, z is depth, and N is nitrogen. The diffusivity term was calculated as:

$$K_\rho(z)=K_0\left\langle\frac{S^4}{S_{GM}^4}\right\rangle$$

after *Gregg* [1989] following the parameterization of *Henyey et al.* [1986]. K_0 was set to 5×10^{-6} m^2 s^{-1} [*Gregg and Kunze*, 1991]; S_{GM}, the Garrett-Munk Shear, was set to $1.66\times10^{-10}\langle (N^2/N_0^2)\rangle^2$; N_0 was 5.2×10^{-3} s^{-1} [*Gregg*, 1989]; and S was the shear measured over 20 m (broadband). A carbon to chlorophyll ratio of 30:1 and a Redfield ratio (C:N) of 6.6:1 were used to convert N to chlorophyll biomass [*Smith et al.*, 1991]. The above diffusion equation was solved analytically for a plane source using the nitrogen gradient defined by Figure 2, with boundary conditions of zero flux above the thermocline and below 160 m and the initial $N_{50\,m}$ set equal to zero. $K_\rho(z)$ values are shown in Figure 8a. Shear within the thermocline peaked on day 249.5 and again from 252 to 254. Modeled biomass increased to >2 mg Chl a m^{-3} in response to the mixing event of 252-254 (Figure 8b). Further biomass increases were noted after day 255, possibly an effect of decreasing buoyancy frequency. These later pulses of biomass were not observed in the data. The peak chl fluorescence value that occurred on day 249.5 was not evident in the modeled data. Either the model poorly represented the mixing regime during this period or another mechanism was responsible for the observed peak on day 249.5. Although the diffusivity model generates believable data, it should only be considered a first-order approximation since the depth distribution of the underwater light field was not taken into account in the estimation of phytoplankton growth. For example, in the model the chlorophyll concentrations were extremely high below 70 m which was a result of the high nutrient flux in the thermocline. If the exponential decaying light field were also accounted for, these chlorophyll values would be reduced. In short, the conversion factor for N:Chl probably does not hold in the thermocline near the base of the euphotic zone.

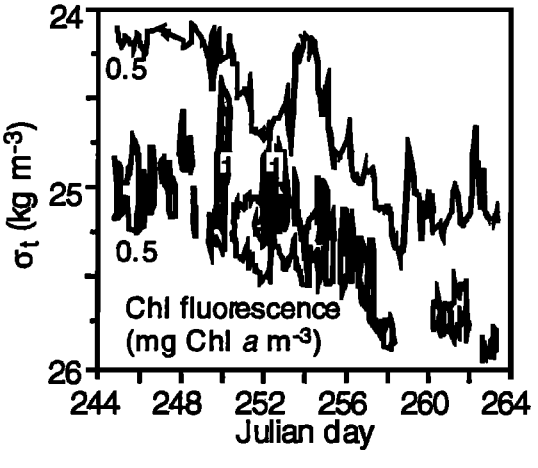

Figure 9. A time series of chl fluorescence distributed across isopycnal surfaces.

Kunze and Sanford [1984] have hypothesized that two sinks for near-inertial wave energy are wave breaking, leading to turbulent mixing, and wave-wave interaction, which shifts wave energy to higher frequencies. Our data also indicate that shear instabilities and intensified turbulence near the front resulted from drastically reduced Richardson numbers in the thermocline on a scale of tens of meters. When plotted on isopycnal surfaces, chlorophyll did not follow the upwelled isopycnals but sloped across several isopycnal surfaces (Figure 9). The smearing of the chl fluorescence signal over several isopycnals is reminiscent of vertical mixing processes which redistribute cells and nutrients over the water column. *Dickey et al.* [1993] described the transition of the phytoplankton community during the late summer of 1987. The euphotic zone and nitracline both deepen corresponding to the seasonal heating cycle. The depth of the DCM followed the trend of the thermocline, which might indicate that phytoplankton in the thermocline were nitrate-limited. It is therefore possible that upwelling of nitrate into the euphotic zone could have stimulated phytoplankton production, enhancing chlorophyll levels in the DCM.

Besides mixing from shear instabilities, which was discussed above, another wave mechanism that could have stimulated phytoplankton growth is wave pumping. For waves with timescales similar to phytoplankton growth rates, wave pumping of isopycnals within or near the nitracline would have lifted nutrients and phytoplankton on isopycnal surfaces into higher light regions, possibly contributing to higher growth rates [*Kamykowski*, 1974, 1976]. However, it is also conceivable that the downward motion of isopycnals might reduce production if the turnover time of cells was increased as a result of lower light conditions. Our data show that as wave energy waxed and waned in the thermocline, isopycnals were displaced downward and upward between the wave troughs and crests at approximately 0.05-0.1 cm s^{-1}. The upwelling of wave crests, however, occurred during the night. Thus peaks in chl fluorescence were not synchronized with solar irradiance as the upwelling occurred. Consequently, peaks in chlorophyll were the result of more than a simple vertical displacement of the phytoplankton into higher light regimes.

The upward and downward displacements of isotherms appeared to coincide with wave periodicity (Plates 1a and1b) even though no clear near-inertial signal was visible in the temperature autospectra. This implies that waves forced the temperature distribution rather than lateral movements of the front. The first chlorophyll increase on day 249.5 could have been the result of advection of a horizontal chlorophyll gradient by near-inertial waves. Near-inertial wave packets

have horizontal length scales of $\lambda_y = (u/2\pi\omega)$; for $\omega = 0.7f$ (day 252) and $u = 60$ cm s^{-1}, $\lambda_y \approx 10$ km. Chlorophyll gradients of 1 mg m^{-3} are not uncommon over 10 km in this region [*Siegel et al.*, 1990]. The first chl fluorescence event lasted ≈ 12 hours, nearly one half the inertial period. The second peak, around day 252, persisted nearly 28 hours (1.3 inertial periods) and approached a 60-km patch size, a bit extreme based on most scaling arguments. Still, it could be argued that the second peak was composed of several small patches generated by the wave oscillations. Because our time series measurements were taken at one point in space, we have a very limited view of horizontal processes, which leads to the difficulty in separating patchiness generated by horizontal wave oscillations from patchiness resulting from mixing events and new production. This is the classic problem of local versus advective effects. Still, the indirect evidence is that mixing was sufficient to upwell nutrients and stimulate new production and that phytoplankton biomass did not follow isopycnal motion since it was not confined to one oscillating isopycnal band, but instead, was distributed across several layers. So, while the first biomass peak might be explained by horizontal advection of the wave, the second peak is better explained by mixing processes.

5. Conclusions

Our observations link wave processes to the temporal variability of the chlorophyll field in the open ocean. It is difficult to specify whether mixing and new production were the cause of two periods of enhanced chlorophyll. Results of a numerical model indicate increased nitrogen flux sufficient to stimulate new production for at least one of the peaks. However, horizontal oscillations in the wave field might also explain phytoplankton patchiness in the wave field.

Inertial waves are common features of the flow field in the Sargasso Sea [*D'Asaro and Perkins*, 1984; *Eriksen*, 1988] and most other ocean sites, which means that episodic mixing forced by waves may be a common phenomenon. If so, perhaps wave-induced patchiness and production are also common phenomena. The effectiveness of inertial waves in causing fertilization pulses will not only depend upon the energy in the waves and the depth to which they penetrate, but also on the depth of the nitracline. High energy waves that propagate downward into the nitracline and mix nutrients upward could stimulate phytoplankton growth if cells were nutrient-limited. Weaker waves would probably lack sufficient energy to inject nutrients into the euphotic zone unless the nitracline shallowed.

Woods [1988] and *Strass* [1992] have suggested that regions of negative vorticity, along fronts 10-40 km in width, can induce upwelling of nutrients and, subsequently, new production. This mechanism is inherently different from that proposed here, in that upward nitracline motions result from asymmetric flow in a frontal jet which reduces vorticity of the flow field [*Onken*, 1992]. Our observations and models also suggest enhanced chl fluorescence in regions along a front, but the source of the patchiness seems to be generated by high-energy inertial waves. Still, these two processes may not be mutually exclusive along fronts.

Acknowledgments. We wish to thank the scientific team involved in collecting Biowatt II data and, particularly, ONR for supporting the research (ONR 00014-89-J-1498). T.C. Granata thanks the Ministerio de Ciencias y Educacion and CSIC, Spain, for support during preparation of the manuscript. The comments of P. Franks and an anonymous reviewer led to improvements in the manuscript and were greatly appreciated.

References

Armstrong, F.A.J., and E.C. La Fond, Chemical nutrient concentrations and their relationship to internal waves and turbidity off Southern California, *Limnol. Oceanogr., 11*(4), 538-547, 1966.

Chereskin, T.K., M.D. Levine, A.J. Harding, and L.A. Regier, Observations of near-inertial waves in acoustic Doppler current profiler measurements made during the Mixed Layer Dynamics Experiment, *J. Geophys. Res., 94*(C6), 8135-8145, 1989.

D'Asaro, E.A., and H. Perkins, A near-inertial internal wave spectrum for the Sargasso Sea in late summer, *J. Phys. Oceanogr., 14*, 489-505, 1984.

Denman, K., and T. Powell, Effects of physical processes on planktonic ecosystems in the coastal ocean, *Oceanogr. Mar. Biol. Annu. Rev., 22*, 125-168, 1984.

Dickey, T., J. Marra, T. Granata, C. Langdon, M. Hamilton, J. Wiggert, D. Siegel, and A. Bratkovich, Concurrent high-resolution bio-optical and physical time seriesobservations in the Sargasso Sea during the spring of 1987, *J. Geophys. Res., 96*(C5),8643-8663, 1991.

Dickey, T., et al., Seasonal variability of bio-optical and physical properties in the Sargasso Sea, *J. Geophys. Res., 98*(C1), 865-898, 1993.

Eriksen, C.C., Variability in the upper-ocean internal wave field at a Sargasso Sea site, *J. Phys. Oceanogr., 18*, 1495- 1513, 1988.

Eriksen, C.C., R.A. Weller, D.L. Rudnick, R.T. Pollard, and L.A. Reiger, Ocean frontal variability in the Frontal Air-Sea Interaction Experiment, *J. Geophys. Res., 96* (C5), 8569-8591, 1991.

Franks, P.J.S., Sink or swim: Accumulation of biomass at fronts, *Mar. Ecol. Prog. Ser., 82*, 1-12, 1992.

Franks, P.J.S., Thin layers of phytoplankton: A model of formation by near-inertial wave shear, *Deep Sea Res., Part I, 42*, 75-91,1995.

Gargett, A.E., and G. Holloway, Dissipation and diffusion by internal waves breaking, *J. Mar. Res., 42*, 15-27, 1984.

Gonella, J., A rotary-component method for analyzing meteorological and oceanographic vector time-series, *Deep Sea Res., 19*, 833-846, 1972.

Gregg, M.C., Scaling turbulent dissipation in the thermocline, *J. Geophys. Res., 94*(C7), 9686-9698, 1989.

Gregg, M.C., and E. Kunze, Shear and strain in Santa Monica Basin, *J. Geophys. Res., 96*(C9), 16,709-16,719, 1991.

Gregg, M.C., E.A. D'Asaro, T.H. Shay, and N. Larson, Observations of persistent mixing and near-inertial internal waves, *J. Phys. Oceanogr., 16*, 856-885, 1986.

Haury, L.R., P.H. Wiebe, M.G. Briscoe, and M.H. Orr, Tidally generated high-frequency internal wave packets and their effects on plankton in Massachusetts Bay, *J. Mar. Res., 41*, 65-112, 1983.

Henyey, F.S., J. Wright, and S.M. Flatte, Energy and action flow through the inertial wave field: An Eikonal approach, *J. Geophys. Res., 91*(C7), 8487-8495, 1986.

Holligan, M., R.D. Pingree, and G.T. Mardell, Oceanic solitons, nutrient pulses and phytoplankton growth, *Nature, 314*, 348-350, 1985.

Kahru, N., Phytoplankton patchiness generated by long internal waves: A model, *Mar. Ecol. Prog. Ser., 10*, 111-117, 1983.

Kamykowski, D., Possible interactions between phytoplankton and semidiurnal internal tides, *J. Mar. Res., 32*, 67-89, 1974.

Kamykowski, D., Possible interactions between phytoplankton and semidiurnal internal tides, II, Deep thermocline and trophic effects, *J. Mar. Res., 34*, 499-509, 1976.

Kundu, P.K., and R.E. Thompson, Inertial oscillations due to a moving front, *J. Phys. Oceanogr., 15*, 1076-1084, 1985.

Kunze, E., Near-inertial wave propagation in geostrophic shear, *J. Phys. Oceanogr., 15*, 544-565, 1985.

Kunze, E., and T.B. Sanford, Observations of near-inertial waves in a front, *J. Phys. Oceanogr., 14*, 566-581, 1984.

Lafleur, P.E., L. Legendre, and A. Cardinal, Dynamique d'une population estuarienne de Diatomees planctoniques: Effet de l'alternance des marees de morte-eau et vive-eau, *Oceanol. Acta, 2*(3), 307-315, 1979.

Levitus, S., Climatological atlas of the world ocean, *NOAA Prof. Pap. 13*, 173 pp., U.S. Govt. Print Off., Washington, D.C., 1982.

Marra, J., et al., The measurement of seasonal primary production from moored optical sensors in the Sargasso Sea, *J. Geophys. Res.*, *97*(C5), 7399-7412, 1992.

McGowan, J.A., and T.L. Hayward, Mixing and oceanic productivity, *Deep Sea Res.*, *25*, 771-793, 1978.

Mied, R.P., C.Y. Shen, C.L. Trump, and G.J. Lindermann, Internal-inertial waves in a Sargasso Sea front, *J. Phys. Oceanogr.*, *16*, 1751-1762, 1986.

Mooers, C.N., Several effects of a baroclinic current on the cross-stream propagation of inertial-internal waves, *Geophys. Astrophys. Fluid Dyn.*, *6*, 245-275, 1975a.

Mooers, C.N., Several effects of a baroclinic current on the three dimensional propagation of inertial-internal waves, *Geophys. Astrophys. Fluid Dyn.*, *6*, 277-284, 1975b.

Munk, W., Internal waves and small-scale processes, in *Evolution of Oceanography*, edited by B.A. Warren and C. Wunsch, pp. 264-291, MIT Press, Cambridge, Mass., 1981.

Onken, R., Mesoscale upwelling and density finestructure in the seasonal thermocline - A dynamical model, *J. Phys. Oceanogr.*, *22*, 1257-1273, 1992.

Pingree, P.D., and G.T. Mardell, Slope turbulence, internal waves and phytoplankton growth at the Celtic Sea shelf-break, *Philos. Trans. R. Soc. Lond. A*, *302*, 663-382, 1981.

Pollard, R.T., On the generation by winds of inertial waves in the ocean, *Deep Sea Res.*, *17*, 795-812, 1970.

Salat, J., J. Tintore, J. Font, D.-P. Wang, and M. Vieira, Near-inertial motion on the shelf-slope front off northeast Spain, *J. Geophys. Res.*, *97*(C5), 7277-7281, 1992.

Siegel, D.A., R. Ituttiaga, R.R. Bidigare, R.C. Smith, H. Pak, T.D. Dickey, J. Marra, and K.S. Baker, Meridional variations of springtime phytoplankton community in the Sargasso Sea, *J. Mar. Res.*, *48*, 379-412, 1990.

Smith, R.C., K.J. Waters, and K.S. Baker, Optical variability and pigment biomass in the Sargasso Sea as determined using deep-sea optical mooring data, *J. Geophys. Res.*, *96*(C5), 8665-8686, 1991.

Smith, S.D., Coefficients for sea surface wind stress, heat flux, and wind profiles as a function of wind speed and temperature, *J. Geophys. Res.*, *93*(C8), 15,467-15,472, 1988.

Stommel, H., Trajectories of small bodies sinking slowly through convection cells, *J. Mar. Res.*, *8*, 24-29, 1949.

Strass, V., Chlorophyll patchiness caused by mesoscale upwelling at fronts, *Deep Sea Res.*, Part A, *39*, 75-96, 1992.

Watts, D.R., Gulf Stream variability, in *Eddies in Marine Science*, edited by A.R. Robinson, pp. 114-144, Springer-Verlag, New York, 1983.

Weller, R.A., The relation of near-inertial motions observed in the mixed layer during the JASIN [1978] experiment to the local wind stress and to a quasi-geostrophic flow field, *J. Phys. Oceanogr.*, *12*, 1122-1136, 1982.

Weller, R.A., Near-surface variability at inertial and subinertial frequencies in the vicinity of the California Current, *J. Phys. Oceanogr.*, *15*, 372-385, 1985.

Weller, R.A., D.L. Rudnick, C.C. Eriksen, K.L. Polzin, N.S. Oakey, J.W. Toole, R.W. Schmitt, and R.T. Pollard, Forced ocean response during the frontal air-sea interaction experiment, *J. Geophys. Res.*, *96*(C5), 8611-8638, 1991.

Woods, J.D., Mesoscale upwelling and primary production, in *Towards a Theory of Biological-Physical Interactions in the World Ocean*, edited by B.J. Rothschild, pp. 7-38, Kluwer Academic, Norwell, Mass., 1988.

T. Dickey and J. Wiggert, Ocean Physics Group, Department of Earth Sciences, University of Southern California, Los Angeles, CA 90089-0740. (e-mail: dickey@usc.edu; jwiggert@usc.edu)

T. Granata, Centro de Estudios Avanzados de Blanes, Cami Santa Barbara, 17300 Blanes, Spain. (email: tim@ceab.es)

(Received July 7, 1994; revised May 8, 1995;
accepted May 31, 1995.)